The Influence of Lateral Carrier Diffusion and Surface Recombination on the Behavior of Semiconductor Optical Amplifier (SOA)-Based MMIs

Jan De Merlier, *Student Member, IEEE*, Geert Morthier, *Senior Member, IEEE*, and Roel Baets, *Senior Member, IEEE*

***Abstract*—The influence of lateral carrier diffusion and surface recombination on the self-imaging properties of semiconductor-optical-amplifier-based multimode interference couplers has been verified by simulations using a beam propagation method. It shows a significant degradation of the self-imaging properties of these devices. Buried heterostructures or deeply etched waveguide structures can decrease the impact when the degree of surface recombination is sufficiently low.**

***Index Terms*—Diffusion, multimode interference coupler (MMI), semiconductor optical amplifier, surface recombination.**

I. Introduction

THE MULTIMODE interference coupler (MMI) has been widely used as a component or subcomponent in a large diversity of devices. It can be used as a switch [1] or simply as a splitter or combiner [2]. The advantage of the MMI as compared to the directional coupler, which can perform analog functions, lies in its robustness toward processing and in its less polarization dependent behavior. This device has also been fabricated in a semiconductor optical amplifier (SOA)-based layer structure in several applications, e.g., high-power lasers [3], regenerators [4], [5], and wavelength converters [6]. However, some side effects, namely lateral carrier diffusion and surface recombination, which result from the active layout, should not be neglected in the design of SOA-based MMIs. The phenomena of lateral carrier diffusion and surface recombination, and their influence on the threshold properties of lasers, have been widely studied. These studies were mainly focussed on the modal gain change [7] and the induced antiguiding effect [8] due to these mechanisms. The self-imaging properties of an MMI are derived from a relationship between the propagation constants of the guided modes resulting from the lateral step-refractive index profile of the MMI waveguide. Therefore, it is not the absolute change of the modal complex propagation constants that is relevant for its operation, but the relative change between the different modes due to the effects mentioned. Perturbations on the lateral step profile can cause a change in the relationship between the propagation constants and degrade the self-imaging properties of the device significantly.

Manuscript received October 29, 2002. The work of J. De Merlier was supported by the Institute for the Promotion of Innovation by Science and Technology (IWT), Flanders.

The authors are with the Department of Information Technology, Ghent University, Ghent, Belgium (e-mail: jan.demerlier@intec.rug.ac.be).

Digital Object Identifier 10.1109/JQE.2003.813191

Using a beam propagation method (BPM), this paper presents simulation results on MMIs, including the two mentioned effects, and demonstrates a serious degradation of the linear behavior of an SOA-based MMI. In Section II, the classical theory of the MMI is briefly recapitulated, with emphasis on the fundamental assumptions and the consequences of lateral carrier diffusion and surface recombination on these assumptions. Section III explains the model that was used in our numerical simulations. Section IV shows simulation results on structures only suffering from the lateral carrier diffusion effect. This is the case for shallowly etched ridge waveguide structures. Section V deals with the combination of lateral carrier diffusion and surface recombination which comes forward in buried heterostructures and deeply etched ridge waveguide structures.

II. Classical Theory of the MMI

Light entering a multimodal waveguide from one of the input waveguides, excites the guided modes. These different modes each propagate with a different propagation constant and due to the interference between all these modes, the lateral light distribution changes as a function of the propagated distance. When a lateral step-refractive index profile is assumed, the lateral wavenumber $k_{y\nu}$ and the propagation constant β_ν of the ν_{th}-order mode are related by the dispersion equation [9]

$$k_{y\nu}^2 + \beta_\nu^2 = k_0^2 n_r^2 \tag{1}$$

with

$$k_0 = \frac{2\pi}{\lambda_0} \quad \text{and} \quad k_{y\nu} = \frac{(\nu+1)\pi}{W_{\text{eff}}} \tag{2}$$

where n_r is the effective index of the ridge, W_{eff} is the effective width of the waveguide including the penetration of the modes in the neighboring material, and λ_0 is the wavelength in vacuum. From these equations, the following relation between the propagation constants can be deduced:

$$\beta_0 - \beta_\nu \simeq \frac{\pi}{3L_\pi}\,\nu(\nu+2) \quad \text{with} \quad L_\pi = \frac{4n_r W_{\text{eff}}^2}{3\lambda}. \tag{3}$$

The length L_π corresponds to the beat length of the two lowest order modes. Based on this relationship, several self-imaging properties can be deduced. However, these properties depend largely on the assumption of a lateral step refractive index profile, as shown in Fig. 1(a). Perturbations of this profile cause a change in the propagation constants of the modes and influence the interference. When an SOA-based MMI is assumed,

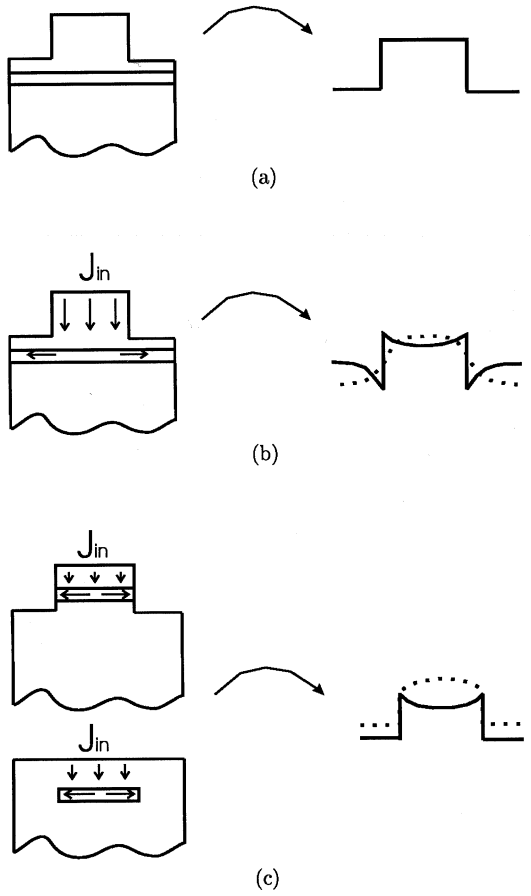

Fig. 1. The waveguide layout, the corresponding lateral refractive index profiles (full lines) and the according carrier density profiles (dotted lines) of: (a) a passive waveguide; (b) an active shallowly etched ridge waveguide structure; and (c) an active buried heterostructure or deeply etched ridge waveguide structure.

carriers are injected into the active layer. These carriers affect the local refractive index in the active layer. This means that when a nonuniform carrier density profile is obtained, the refractive index profile is no longer step-like. A shallowly etched SOA-waveguide will suffer from lateral carrier diffusion away from the ridge. This results in a nonuniform carrier density profile and gives a perturbation as shown in Fig. 1(b). In the case of a "finite" active layer width, surface recombination will induce a diffusion current toward the edges of the active layer. This results in a refractive index perturbation as given in Fig. 1(c).

III. Simulation Program

The simulation program consists of a finite difference beam propagation method (FD-BPM) which takes care of the propagation of the light and has been linked to a program which calculates the lateral carrier density profile taking into account the interaction between the light and the carriers, through stimulated emission, and among the carriers. Although the latter program implies the solution of the 2-D current continuity equations, it can be reduced to a one dimensional problem by noting that the thickness of the active layer is very small as compared to the diffusion length. Therefore the timescale in which the carriers diffuse in the direction orthogonal to the active layer is an order of magnitude faster than the lateral diffusion. The lateral current consists of a drift current, due to the field induced by the different electron and hole distribution, and out of a diffusion current induced by the nonuniform distribution of the carriers. All of these effects can be represented by the effective diffusion coefficient [10]. Eventually, the approximated steady-state rate equation can be expressed as follows:

$$\frac{J}{qd} - D_{\text{eff}}\frac{\partial^2 N}{\partial x^2} - AN - BN^2 - CN^3 - \frac{\Gamma a(N-N_0)P(x)}{\hbar\omega d} = 0 \quad (4)$$

Here, J is the current density, q is the elementary charge, d is the thickness of the active layer, D_{eff} is the effective diffusion coefficient, A, B, and C are the nonradiative, radiative, and Auger recombination coefficients, respectively, $\hbar$ is the reduced Planck constant, ω is the optical angular frequency, and $P(x)$ is the lateral power density profile. This equation has been solved using a transfer matrix method. The solution allows us to calculate the modified lateral complex refractive index profile

$$n(x) = n_r + \Gamma\left(\beta N(x) + i\frac{a}{2k_0}(N(x)-N_0)\right) \quad (5)$$

where n_r is the effective refractive index of the ridge, Γ is the confinement factor, β is the antiguiding factor, $N(x)$ is the carrier density, a is the differential gain, k_0 is the wave vector, and N_0 is the transparency electron density.

TABLE I
Parameter Values

Parameter	Value
effective index ridge	3.23
effective index cladding	3.17
Differential gain	$2.7\ 10^{-16} cm^2$
Thickness active layer	0.15 μm
Confinement factor	0.33
Unimolecular recombination coefficient	$1.67\ 10^{8} s^{-1}$
Transparency electron density	$10^{18}\ cm^{-3}$
Bimolecular recombination coefficient	$10^{-10}\ cm^3 s^{-1}$
wavelength	1.55 μm
Auger recombination coefficient	$6\ 10^{-29} cm^6 s^{-1}$
anti-guiding factor	$-1.8\ 10^{-20} cm^3$
propagation losses	$20\ cm^{-1}$

IV. Lateral Carrier Diffusion

Due to the lack of potential barriers beneath the edges of a shallowly etched ridge waveguide structure, the carriers can diffuse away from the guiding ridge. This causes the carrier density profile to be a clock shape. The shape is mainly determined by the value of the effective diffusion coefficient. The value of this parameter depends on the used material and on the substrate doping [10]. Therefore, this parameter has been swept. A typical value for D_{eff} in the InGaAsP–InP material system is 10 cm^2/s for an n-type substrate. The other relevant parameter values are listed in Table I and are fixed for all simulations. Fig. 2 shows the calculated profile for different values of D_{eff} and a fixed current density of 6 kA/cm^2. As the diffusion coefficient increases, the shape deviates more and more. This is due to the fact that the perturbation spreads over the diffusion

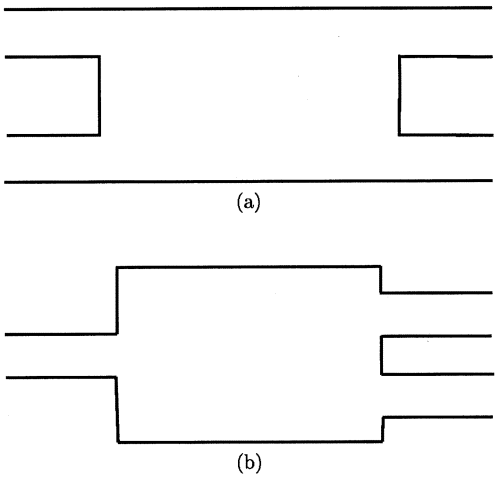

Fig. 2. Carrier density profile for different values of the effective diffusion coefficient D_{eff}.

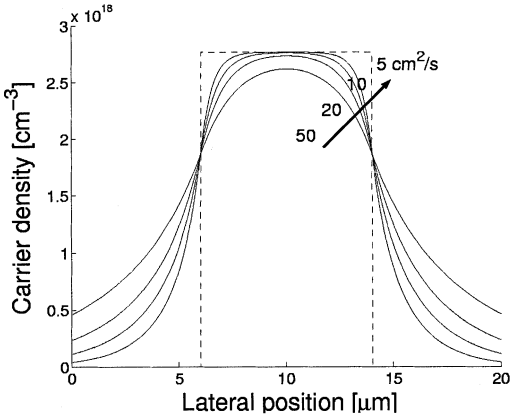

Fig. 3. Layout 2×2 MMI and 1×2 MMI.

length L_{diff}, which equals $\sqrt{D_{\text{eff}}\tau}$, with τ being the carrier lifetime, into the waveguide. Increasing D_{eff} implies a larger perturbation. Due to the fixed region where the perturbation is significant, independent of the width of the waveguide, the effect on the refractive index profile will increase as the MMI width gets narrower. Increasing the waveguide width would decrease the impact but as the surface area of an MMI rises with the cube of the width, as is clear from (3), this would significantly increase the required current. Furthermore, as the width of the MMI increases, the component becomes more sensitive to the tolerance in width [9].

Simulations have been done for a shallowly etched 2×2 MMI-SOA with a layout as in Fig. 3(a). The MMI width equals 8 μm and the input and output waveguides are 3 μm in width. This device has the property of 3-dB coupling at a distance of $3L_\pi/2$ to the two output waveguides and total coupling to the output waveguide in the cross state at twice that distance. The applied current density equals 6 kA/cm^2 for all simulations, unless otherwise stated.

The ideal behavior, where the carrier density is uniform under the ridge, has been simulated and plotted in Fig. 4. In the figure, the coupling to the fundamental mode in the bar and cross output waveguides are plotted as a function of the MMI length. It is clear that, in this case, the device behaves properly and the gain

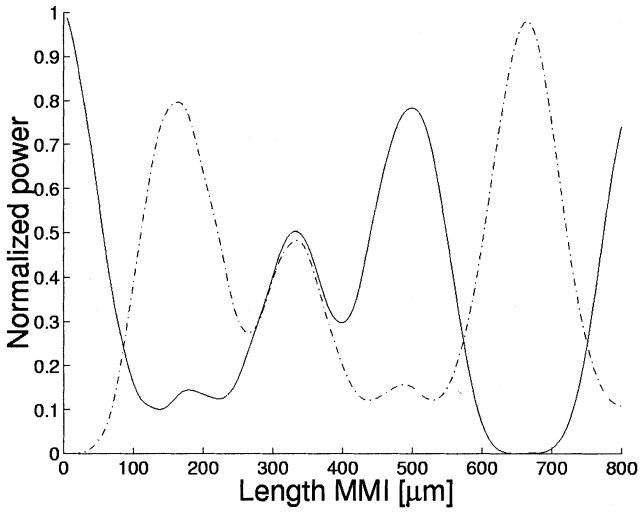

Fig. 4. Normalized power in bar and cross state as a function of the length for an ideal active waveguide.

has a negligible impact. Perfect 3-dB coupling is obtained for a length of 330 μm and total coupling to the cross state output waveguide after 660 μm.

In Fig. 5(a)–(d), simulation results for different values of D_{eff} are plotted. As the diffusion coefficient increases, the self-imaging properties move further away from the ideal MMI. It becomes clear that at the "ideal" 3 dB-length there is a large imbalance between both outputs which can mount up to 4.5 dB. An efficient self imaging is obtained to the bar-state output after a propagation distance of 520 μm and becomes more significant as D_{eff} increases. In Fig. 6, the normalized power in the bar and the cross state is shown for current densities of 1 kA/cm^2, 6 kA/cm^2 and 12 kA/cm^2 using a fixed effective diffusion coefficient of 10cm^2/s. As can be seen from this figure, the influence of the current on the self-imaging properties is only marginal.

Also, for a 1×2 MMI-SOA, with a layout given in Fig. 3(b), simulations have been performed. In this case, the input waveguide is positioned at the center of the multimodal waveguide. This implies that only the even modes will be excited and results in self-imaging properties at reduced distances as compared to the previous device. For a length of $3L_\pi/8$, 3-dB splitting is obtained. The MMI width equals 8 μm and the input and output waveguides are 2.5 μm in width. The spacing between the centers of the two output waveguides is 4 μm. For this device, the 3-dB length equals 85 μm, as is clear from the simulations given in Fig. 7. Total coupling to the output waveguide, located in the center of the MMI output, is obtained at twice that distance. The simulation results show that, when lateral carrier diffusion is taken into account, the ideal 3-dB splitting point is shifted toward longer lengths, but the component can still work properly. This is due to the shorter length of the device, which limits the accumulation of the phase mismatch between the modes.

V. Surface Recombination

In order to avoid the lateral current spreading, a buried heterostructure or a deeply etched ridge waveguide structure can

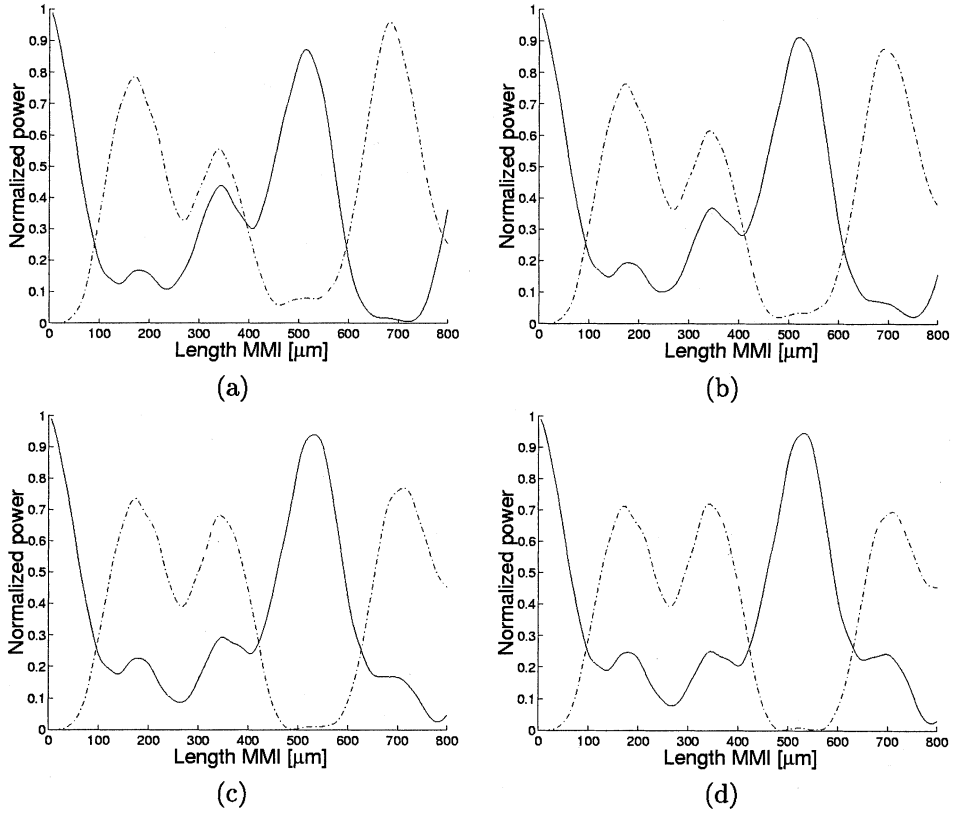

Fig. 5. Normalized power in bar and cross state as a function of the length for $D_{\text{eff}} =$: (a) 5; (b) 10; (c) 20; and (d) 50 cm^2/s.

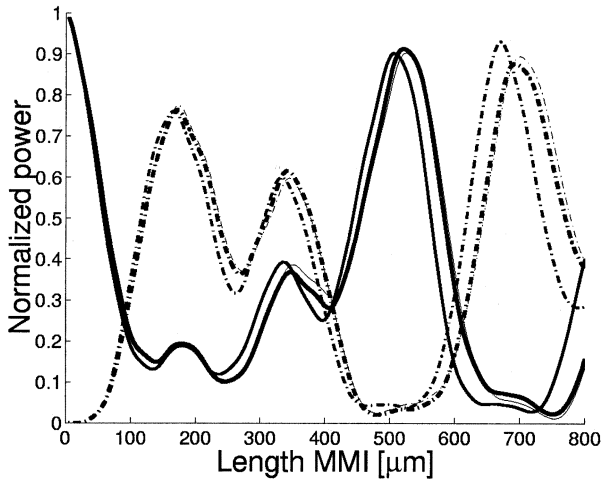

Fig. 6. Normalized power in bar and cross state as a function of the length for current densities 1 kA/cm^2 (thick lines), 6 kA/cm^2 (normal lines), and 12 kA/cm^2 (thin lines).

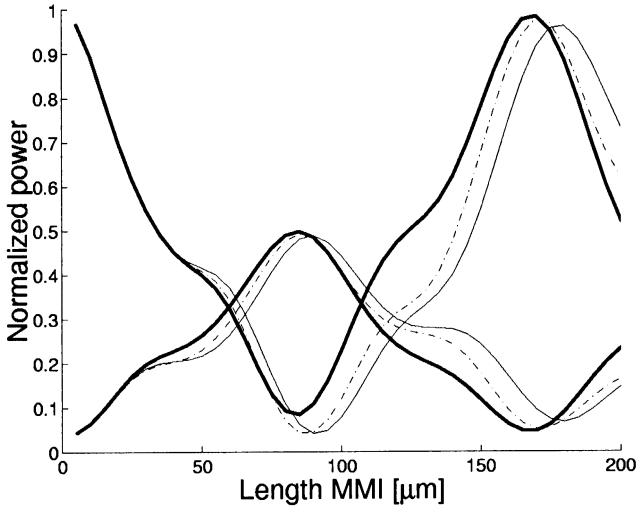

Fig. 7. Normalized power in output waveguide as a function of the length for central position and 3 dB position. Thick lines: results for the ideal case. Normal lines: results for $S = 10^5$ cm/s. Dashed lines: results for a $D_{\text{eff}} = 50$ cm^2/s.

be used. In this case, the lateral current will be confined but the surface recombination at the edges of the active layer will determine the carrier density profile. A fixed effective diffusion coefficient of 10 cm^2/s has been used for these simulations. The carrier density distributions are plotted as a function of the surface recombination rate in Fig. 8. The nonuniformity is negligible for values lower than 10^4 cm/s. The impact on the behavior of the 2×2 MMI is shown in Fig. 9(a) and (b) for the different values of surface recombination. For a value of 10^4 cm/s, the impact is still moderate but for higher surface recombination rates, the influence increases tremendously. This is clear from the simulation results for $S = 10^5$ cm/s. It can be concluded that the surface recombination should be lower than 10^4 cm/s in order to have negligible influence on the self-imaging behavior. It should be noted that the surface recombination rate is highly dependent on the material system. Typical values for the InGaAsP–InP system are 1–2 $10^4 cm/s$ [12]. An additional wet-etching step can be introduced in the fabrication process in order to decrease the etching damage and contamination due to

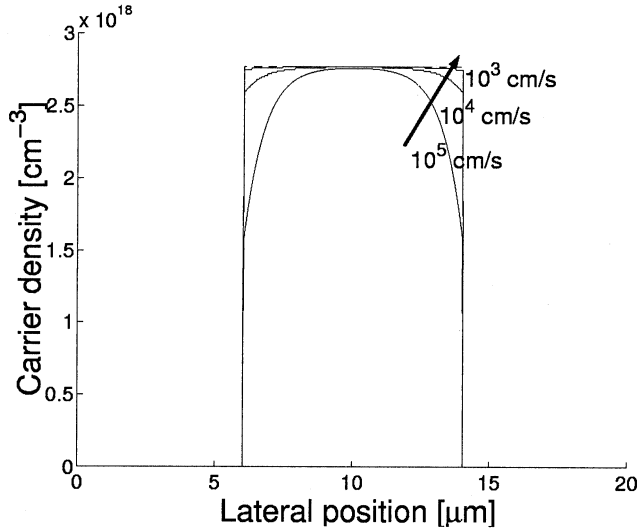

Fig. 8. Carrier density profile for different values of surface recombination parameter S.

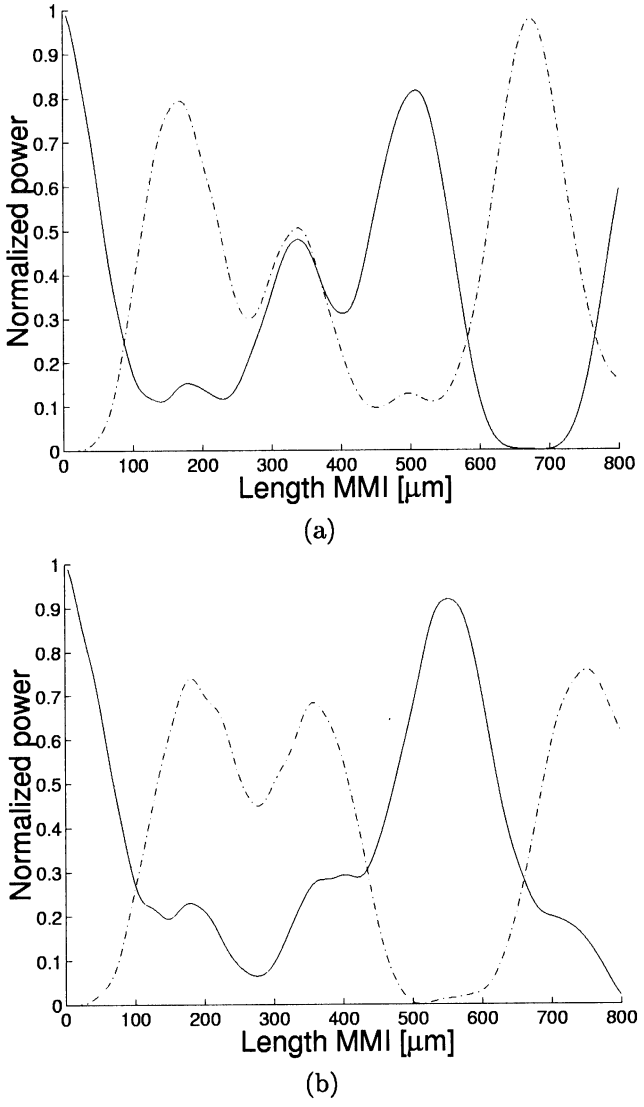

Fig. 9. Normalized power in bar and cross state as a function of the length for (a) 10^4 and (b) 10^5 cm/s.

the dry etching. For the InGaAs–GaAs system, the value can mount up to more than 10^6 cm/s [11], in which case the device perofrmance will suffer a lot from this effect. Simulation results for the 1×2 MMI for $S = 10^5$ cm/s are plotted in Fig. 7. As in the case of a shallowly etched waveguide structure, these simulations reveal no significant degradation.

VI. Conclusion

Simulations have shown the significant effect of lateral carrier diffusion and surface recombination in the active layer on the self-imaging properties of SOA-based MMIs. This effect can be minimized by using buried heterostructures or deeply etched ridge waveguide structures. In this case, the surface recombination must be kept below 10^4 cm/s, which is possible for the InGaAsP–InP material system when special care is taken of the etching process. However, this value can probably not be reached in, e.g., the InGaAs–GaAs material system. Simulation results on a 1×2 MMI, based on restricted interference, show no significant degradation due to the decreased self-imaging distance.

Acknowledgment

J. De Merlier thanks D. Van Thourhout for the useful discussions.

References

[1] S. Nagai, G. Morishima, H. Inayoshi, and K. Utaka, "Multimode interference photonic switches (MIPS)," *J. Lightwave Technol.*, vol. 20, pp. 675–681, Apr. 2002.

[2] K. Kudo, K. Yashiki, T. Sasaki, Y. Yokoyama, K. Hamamoto, T. Morimoto, and M. Yamaguchi, "1.55 μm wavelength-selectable microarray DFB-LD's with monolithically integrated MMI combiner, SOA, and EA-modulator," *IEEE Photon. Technol. Lett.*, vol. 12, pp. 242–244, Mar. 2000.

[3] K. Hamamoto, E. Gini, C. Holtmann, H. Melchior, S. Sudo, K. Mori, T. Sasaki, and M. Yamaguchi, "Active multi-mode-interferometer semiconductor optical amplifier," *Electron. Lett.*, vol. 36, pp. 1218–1220, 2000.

[4] J. De Merlier, G. Morthier, S. Verstuyft, T. Van Caenegem, I. Moerman, P. Van Daele, and R. Baets, "Experimental demonstration of all-optical regeneration using an MMI-SOA," *IEEE Photon. Technol. Lett.*, vol. 14, pp. 660–662, May 2002.

[5] J. De Merlier, G. Morthier, P. Van Daele, I. Moerman, and R. Baets, "All-optical 2R regeneration based on integrated asymmetric Mach–Zehnder interferometer incorporating MMI-SOA," *Electron. Lett.*, vol. 38, pp. 238–239, Feb. 2002.

[6] C. Janz, F. Poingt, F. Pommereau, W. Grieshaber, F. Gaborit, D. Leclerc, I. Guillemot, and M. Renaud, "All-active dual-order mode (DOMO) Mach–Zehnder wavelength converter for 10 Gbit/s operation," *Electron. Lett.*, vol. 35, pp. 1862–1863, Oct. 1999.

[7] S. Y. Hu, S. W. Corzine, K.-K. Law, D. B. Young, A. C. Gossard, L. A. Coldren, and J. L. Merz, "Lateral carrier diffusion and surface recombination in InGaAs/AlGaAs quantum well ridge-waveguide lasers," *J. Appl. Phys.*, vol. 76, pp. 4479–4487, 1994.

[8] M.-C. Amann and Stegmüller, "Threshold current analysis of InGaAsP/InP," *Proc. Inst. Elect. Eng.*, vol. 133, pp. 341–348, 1986.

[9] L. B. Soldano and E. C. M. Pennings, "Optical multi-mode interference devices based on self-imaging: Principles and applications," *J. Lightwave Technol.*, vol. 13, pp. 615–627, Apr. 1995.

[10] W. B. Joyce, "Carrier transport in double heterostructure active layers," *J. Appl. Phys.*, vol. 53, pp. 7235–7239, 1982.

[11] V. Malyarchuk, J. W. Tomm, V. Talalaev, Ch. Lienau, F. Rinner, and M. Baeumler, "Nanoscopic measurements of surface recombination velocity and diffusion length in a semiconductor quantum well," *Appl. Phys. Lett.*, vol. 81, pp. 346–348, July 2002.

[12] T. Baba, K. Inoshita, H. Tanaka, J. Yonekura, M. Ariga, A. Matsutani, T. Miyamoto, F. Koyama, and K. Iga, "Strong enhancement of light extraction efficiency in GaInAsP 2-D-arranged microcolumns," *J. Lightwave Technol.*, vol. 17, pp. 2113–2119, Nov. 1999.

Jan De Merlier (S'03) received the physical engineering degree in 1998 from Ghent University, Ghent, Belgium, where he is currently working toward the Ph.D. degree in electrical engineering in the Department of Information Technology.

His main research interests are the dynamic properties of semiconductor optical amplifiers for use in all-optical regenerators.

Geert Morthier (M'93–SM'01) received the degree in electrical engineering in 1987 and the Ph.D. degree in 1991, both from the University of Ghent, Ghent, Belgium.

Since 1991, he has been a member of the permanent staff of the Interuniversity Microelectronics Center (IMEC). From 1998 to 1999, he was the Project Manager of the ACTS project ACTUAL dealing with the control of widely tunable diodes. Since 2001, he has been the Project Manager of the IST project NEWTON, which focuses on new widely tunable lasers. In 2001, he was appointed part-time Professor at the University of Ghent. His main interests are in the modeling and characterization of optoelectronic components. He has authored or co-authored around 100 papers in the field. He is also a co-author of the *Handbook of Distributed Feedback Laser* (Norwood, MA: Artech House, 1997) and co-editor of the book *How to Model and Measure Photonic Components: Experience from a European Project* (New York: Springer-Verlag, 1998).

Roel Baets (M'88–SM'96) received the degree in electrical engineering from Ghent University, Ghent, Belgium, in 1980, the M.Sc. degree in electrical engineering from Stanford University, Stanford, CA, in 1981, and the Ph.D. degree from Ghent University in 1984.

Since 1981, he has been with the Department of Information Technology (INTEL) of Ghent University, and since 1989, a Professor in the Engineering Faculty. From 1990 to 1994, he was a part-time Professor at the Technical University of Delft, The Netherlands. He has mainly worked in the field of photonic components. With about 300 publications and conference papers and ten patents, he has made contributions to the design and fabrication of III–V semiconductor laser diodes, passive guided wave devices, photonic ICs, and microoptic components. He leads the Optoelectronic Components and Systems group at Ghent University-INTEL (which is an associated lab of IMEC), working on photonic devices for optical communication and optical interconnect.

Dr. Baets is a member of the Optical Society of America, IEEE LEOS, SPIE, and the Flemish Engineers Association. He has been member of the program committees of OFC, ECOC, the IEEE Semiconductor Laser Conference, ESSDERC, CLEO-Europe, and the European Conference on Integrated Optics. He has been Chairman of the IEEE LEOS Benelux chapter from 1999 to 2001. Currently, he is a member of the Board of Governors of IEEE /LEOS.